

RESEARCH

Open Access



# Investigation of rectangular apertures and their application on speckle imaging

A. M. Hamed<sup>1\*</sup>  and T. A. Al-Saeed<sup>2</sup>

## Abstract

**Background:** An aperture in the form of four squares arranged symmetrically along the cartesian coordinates with equal distances from the center investigated. Three models are suggested in the computation of the Point Spread Function PSF using the FFT technique. In the 1st model, circular annulus is placed in the center, while in the 2nd model a square annulus is shown, and in the 3<sup>rd</sup> model, two symmetric squares in the models 1, 2 are replaced by two symmetric rectangles while the center remains of square annulus. In all the models, central obstruction is made seeking to improve the PSF.

**Results:** An analytical formula for the PSF for the aperture described in the 1st model is obtained. In addition, the autocorrelation corresponding to these apertures are computed and compared with the known autocorrelation corresponding to the whole square aperture. An application on speckle imaging is given using these apertures combined with the diffuser. All images for the design of the apertures and the speckle images are made using the MATLAB code.

**Conclusions:** The resolution computed from the FWHM showed an improvement for the suggested square apertures as compared with the uniform square aperture where the total width is kept constant. In addition, the strength of the legs in the PSF for the suggested apertures is much higher than that corresponding the uniform aperture which makes it useful for imaging of extended objects.

**Keywords:** Modulated square apertures, Point spread function, Speckle images

## 1 Background

Speckle can be explained using the Hugen's principle by considering the microscopic structure of the surface [1]. Since 1948 before the advent of laser, the aperture filtering suggested annular shape for the sake of resolution improvement realized by many authors like in [2–11].

Aperture filtering methods proposed and investigated in 1983 where linear and quadratic apertures are studied in [12, 13]. Recently, a linear-quadratic arrangement is investigated in [14]. Different applications on speckle microscopic and medical images are investigated by the author using different filtering apertures e.g., in [15–17]. Novel

techniques for the generation of customized speckle with a tailored speckle-size distributions are presented in [18–20].

Recently, design of microelectromechanical systems (MEMS) devices with rectangular optical apertures was fabricated and used for the detection of transparent biological cells [21]. An interesting recent work provides that different approaches of mathematical modeling are considered in [21, 22]. For example, dynamic behavior of two predators-one prey model with generalized functional response and time-fractional derivative is outlined and discussed in [21].

In this paper, we propose new rectangular arrangement of apertures of two-fold symmetry with annular central disc, and we compute the PSF and the autocorrelation corresponding to these apertures. In addition, an application on speckle imaging modulated by the aperture is given. Theoretical analysis, results and discussion are followed by a conclusion.

\*Correspondence: amhamed73@hotmail.com

<sup>1</sup> Physics Department, Faculty of Science, Ain Shams University, Cairo, Egypt

Full list of author information is available at the end of the article

## 2 Methods

A rectangular aperture composed of four equal squares placed at equal distances from the center. The total matrix of rectangular shape has dimensions  $1024 \times 1024$  pixels. While, the dimensions of each square  $(x_0, y_0) = 128 \times 128$  pixels and located along the cartesian coordinates  $(x, y)$  at distances  $\pm x_d$  and  $\pm y_d$  as shown in the Fig. 1a. A central obstruction is governed by the difference between two circles where the width of the annulus = 32 pixels. A uniform illumination emitted from laser beam is incident upon this new aperture, hence the amplitude transmittance is written as follows:

$$A(x, y) = \text{rect}(x - x_d, y) + \text{rect}(x + x_d, y) + \text{rect}(x, y - y_d) + \text{rect}(x, y + y_d) + \text{circ}(r_1) - \text{circ}(r_2) \quad (1)$$

where

$$\text{rect}(x, y) = 1; \left| \frac{x}{x_0} \right| \leq 1, \left| \frac{y}{y_0} \right| \leq 1,$$

$$\text{circ}(r_1) = 1; \left| \frac{r}{r_{01}} \right| \leq 1, \quad \text{and} \quad \text{circ}(r_2) = 1; \left| \frac{r}{r_{02}} \right| \leq 1$$

The Point Spread Function (PSF) corresponding to the novel aperture described by Eq. (1) is obtained by operating the Fourier transform as follows:

The 1st transformation is solved taking in consideration that convolution of two functions is equivalent to simple product of the F.T. of each function, hence we write:

$$F.T.\{\text{rect}(x, y) \otimes \delta(x - x_d, y)\} = F.T.\{\text{rect}(x, y)\} \cdot F.T.\{\delta(x - x_d, y)\}$$

It is known that the Fourier transform of rect function is written as:

$$F.T.\{\text{rect}(x, y)\} = x_0 y_0 \left[ \frac{\sin\left(\frac{\pi x_0 u}{\lambda f}\right)}{\left(\frac{\pi x_0 u}{\lambda f}\right)} \right] \left[ \frac{\sin\left(\frac{\pi y_0 v}{\lambda f}\right)}{\left(\frac{\pi y_0 v}{\lambda f}\right)} \right] = x_0 y_0 \text{sinc}(x') \text{sinc}(y') \quad (3)$$

where sinc function is defined as:

$\text{sinc}(x') = \sin(\pi x') / \pi x'$ ,  $x' = x_0 u / \lambda f$ , and a similar expression for  $\text{sinc}(y')$ .

Also, the Fourier transform of circ function as obtained as follows [11]:

$$F.T.\{\text{circ}(r_1)\} = 2J_1(Z_1)/Z_1, \quad \text{and} \quad F.T.\{\text{circ}(r_2)\} = 2J_1(Z_2)/Z_2 \quad (4)$$

where  $Z_1 = 2\pi r_{01} w_1 / \lambda f$  and  $Z_2 = 2\pi r_{02} w_2 / \lambda f$  represent the reduced coordinates in the Fourier planes corresponding to the external and internal circles of radii  $r_{01}$  and  $r_{02}$ .  $w_{1,2} = \sqrt{u^2 + v^2}$  is the radial coordinate in the Fourier plane corresponding to each circle.

The Fourier transform of shifted dirac-delta function gives inclined plane wave as:

$$\begin{aligned} F.T.\{\delta(x - x_d, y)\} &= \iint_{-\infty}^{\infty} \{\delta(x - x_d, y)\} \exp\left[-\frac{j2\pi}{\lambda f}(xu + yv)\right] dx dy \\ &= \exp\left(-\frac{j2\pi x_d u}{\lambda f}\right) \iint_{-\infty}^{\infty} \{\delta(x - x_d, y)\} \exp\left[-\frac{j2\pi}{\lambda f}((x - x_d)u + yv)\right] dx dy \\ &= \exp\left(-\frac{j2\pi x_d u}{\lambda f}\right) \end{aligned} \quad (5)$$

$$\begin{aligned} h(x, y) &= F.T.\{A(x, y)\} \\ &= F.T.\{\text{rect}(x - x_d, y) + \text{rect}(x + x_d, y) + \text{rect}(x, y - y_d) + \text{rect}(x, y + y_d) + \text{circ}(r_1) - \text{circ}(r_2)\} \\ &= F.T.\{\text{rect}(x, y) \otimes \delta(x - x_d, y)\} + F.T.\{\text{rect}(x, y) \otimes \delta(x + x_d, y)\} \\ &\quad + F.T.\{\text{rect}(x, y) \otimes \delta(x, y - y_d)\} + F.T.\{\text{rect}(x, y) \otimes \delta(x, y + y_d)\} \\ &\quad + F.T.\{\text{circ}(r_1)\} - F.T.\{\text{circ}(r_2)\} \end{aligned} \quad (2)$$

Similar expressions are obtained for the other shift of the dirac-delta function as follows:

$$F.T.\{\delta(x + x_d, y)\} = \exp\left(+\frac{j2\pi x_d u}{\lambda f}\right) \quad (6)$$

$$F.T.\{\delta(x, y - y_d)\} = \exp\left(-\frac{j2\pi y_d v}{\lambda f}\right) \quad (7)$$

$$F.T.\{\delta(x, y + y_d)\} = \exp\left(+\frac{j2\pi y_d v}{\lambda f}\right) \quad (8)$$

Plugging Eqs. (3–8) in Eq. (2), we get:

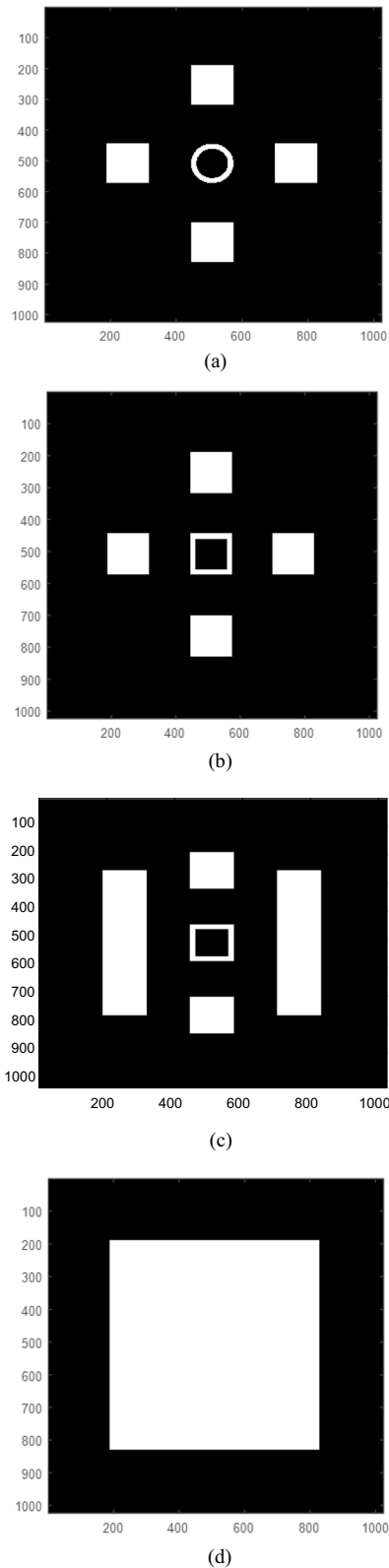


**Fig. 1** **a** An aperture composed of four squares arranged symmetrically along the cartesian coordinates and obstructed by a circular annulus placed in the center of diameter 128 pixels and annular width 16 pixels. Each square has dimensions 128 x 128 pixels compared with the whole matrix of dimensions 1024 x 1024 pixels. **b** An aperture composed of four squares arranged symmetrically along the cartesian coordinates and obstructed by a square annulus placed in the center of width 16 pixels. Each square has dimensions 128 x 128 pixels and shifted by 256 pixels along the coordinates. **c** An aperture composed of two squares arranged symmetrically along the y-axis, and two rectangles arranged along x-axis and obstructed by an annular rectangle placed in the center. Each square has dimensions 128 x 128 pixels and shifted by 256 pixels along the coordinates, and each rectangle has dimensions 128 x 512 pixels and shifted by  $\pm 256$  pixels from the x-axis. **d** An aperture composed of a square of dimensions 640 x 640 pixels

$$h(x, y) = x_0 y_0 \text{sinc}(x') \text{sinc}(y') + \left\{ \exp\left(-\frac{j2x_d u}{f}\right) + \exp\left(+\frac{j2x_d u}{f}\right) + \exp\left(-\frac{j2y_d v}{f}\right) + \exp\left(+\frac{j2y_d v}{f}\right) \right\} + \left\{ \frac{2J_1(Z_1)}{Z_1} - \frac{2J_1(Z_2)}{Z_2} \right\} \quad (9)$$

Hence, the PSF is finally written as follows:

$$h(x, y) = 2x_0 y_0 \text{sinc}(x') \text{sinc}(y') \left\{ \cos\left(\frac{2x_d u}{f}\right) + \cos\left(\frac{2y_d v}{f}\right) \right\} + \left\{ \frac{2J_1(Z_1)}{Z_1} - \frac{2J_1(Z_2)}{Z_2} \right\} \quad (10)$$

Equation (10) is rewritten as follows:

$$h(x, y) = 4x_0 y_0 \text{sinc}(x') \text{sinc}(y') \left\{ \cos\left(\frac{(x_d u + y_d v)}{f}\right) \cos\left(\frac{(x_d u - y_d v)}{f}\right) \right\} + \left\{ \frac{2J_1(Z_1)}{Z_1} - \frac{2J_1(Z_2)}{Z_2} \right\} \quad (11)$$

The intensity impulse response is computed from the modulus square of Eq. (11) as follows:

$$\begin{aligned}
I(x, y) &= 16x_0^2y_0^2\text{sinc}^2(x')\text{sinc}^2(y') \left\{ \cos^2\left(\frac{(x_d u + y_d v)}{f}\right) \cos^2\left(\frac{(x_d u - y_d v)}{f}\right) \right\} \\
&+ 8x_0y_0\text{sinc}(x')\text{sinc}(y') \left\{ \cos\left(\frac{(x_d u + y_d v)}{f}\right) \cos\left(\frac{(x_d u - y_d v)}{f}\right) \right\} \\
&\left\{ \frac{2J_1(Z_1)}{Z_1} - \frac{2J_1(Z_2)}{Z_2} \right\} + \left\{ \frac{2J_1(Z_1)}{Z_1} - \frac{2J_1(Z_2)}{Z_2} \right\}^2
\end{aligned} \tag{12}$$

### 3 Results

The design of the new apertures is shown in the Fig. 1. It is fabricated using a MATLAB code. The aperture composed of four squares arranged symmetrically along the cartesian coordinates and obstructed by an annulus placed in the center is shown as in the Fig. 1a. Each square has dimensions  $128 \times 128$  pixels compared with the whole matrix of dimensions  $1024 \times 1024$  pixels. The total effective aperture in the whole matrix has dimensions of  $640 \times 640$  pixels. Similar aperture is shown in the Fig. 1b while the circular annulus is replaced by square annulus. In addition, an aperture of two symmetric squares arranged along  $y$ -axis, and two symmetric rectangles placed along  $x$ -axis where the center remains of square annulus that is shown in the Fig. 1c. An effective square aperture of dimensions  $640 \times 640$  pixels is shown in the Fig. 1d.

The PSF corresponding to the apertures under investigation are computed using the FFT technique. The plot of the PSF in the range from 460 pixels up to 560 pixels is shown in the Fig. 2a for the 1st model, while Fig. 2b represents the PSF for the 2nd model, and the Fig. 2c for the PSF for the 3rd model. A comparative result for the PSF corresponding to the effective square is shown in the Fig. 2d.

A magnified portion of the plot is shown in the range from 500 pixels up to 526 pixels as in the Fig. 3a–C Fig. 2a–c. The image of the diffraction for the aperture shown in the Fig. 1a is plotted as in the Fig. 4. It is named as the intensity Fourier spectrum or intensity impulse response equals the modulus square of the PSF corresponding to the aperture.

The speckle image in presence of the aperture shown in L.H.S., while in the R.H.S., speckle image in absence of the aperture is represented as in the Fig. 5a.

The corresponding line plots are shown as in the Fig. 5b. The range taken is from 60 up to 120 pixels for both line plots.

The autocorrelation of the apertures shown in the Fig. 1a–d are computed and plotted as shown in the Fig. 6a–d, where the total band width = 1280 pixels which is two times the aperture width of 640 pixels.

### 4 Discussion

It is shown, referring to the Figs. 2 and 3, that the full width at half-maximum (FWHM) is the same for the suggested models, shown in the Fig. 1, and equals to 1 pixels as compared with the FWHM for the effective aperture which equals 3 pixels. Hence, resolution improvement is attained using the suggested designs of apertures shown in the Fig. 1a–c. The difference between the 1st two models and the 3rd model is apparent in the strengthen of the legs shown in the Fig. 2c as compared with the legs shown in the Fig. 2a, b. In all cases, as shown in the Fig. 2a–c, the strength of the legs of the diffraction pattern (PSF) is considered useful for imaging of extended objects as compared with the weak strength obtained in Fig. 2d.

The magnified portions representing the PSF corresponding to the different models shown in the Fig. 3, is for the discrimination of the PSF structure.

The image of the diffraction from the aperture shown in the Fig. 4 is called the intensity impulse response or the modulus square of the PSF.

The speckle image formed in presence of the aperture using certain diffuser as a randomly distributed function is obtained by applying the Fourier transform (F.T.) upon the multiplication of the aperture and the diffuser illuminated by uniform amplitude emitted from spatially filtered laser beam. Hence, the formed speckle image is the convolution product of the PSF for the aperture and the F.T. corresponding to the diffuser. While the other speckle image shown in the R.H.S. is simply the F.T. corresponding to the same diffuser as in the Fig. 5a.

It is shown that the plots corresponding to the speckle images are different Fig. 5b. In addition, the contrast is

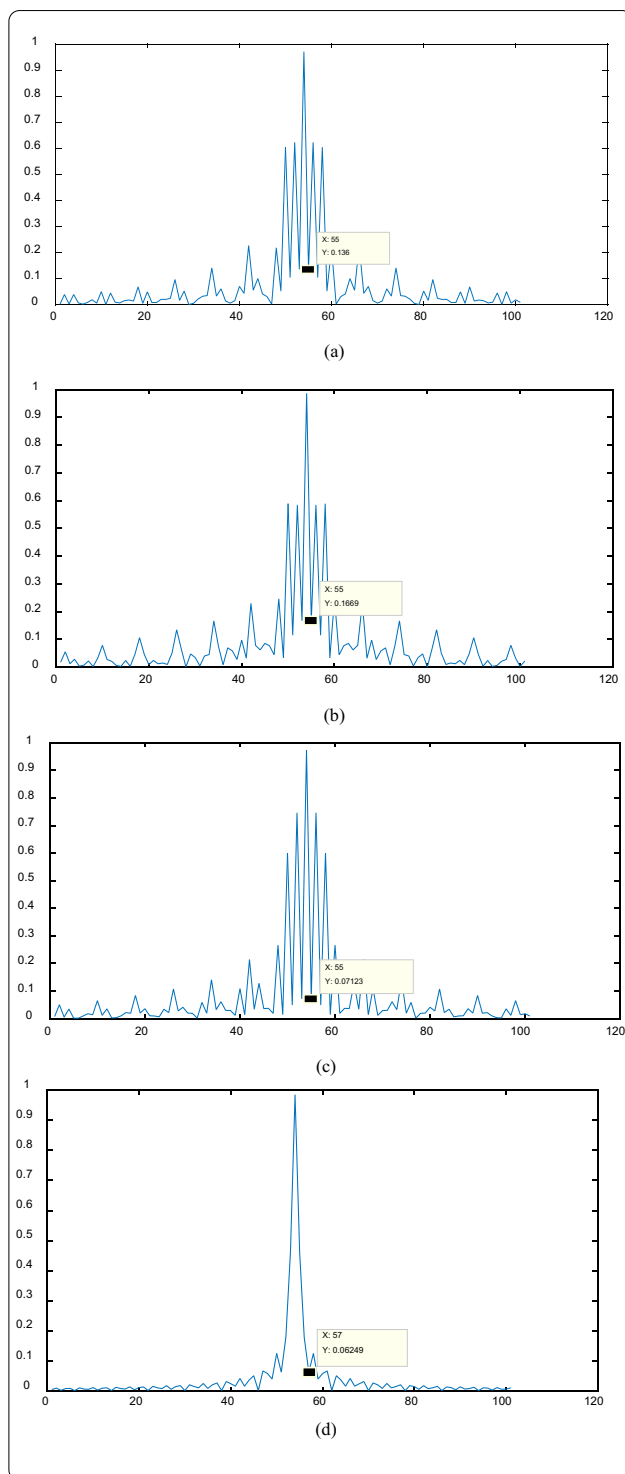


**Fig. 2** **a** The PSF for the aperture shown in the Fig. 1a, in the range from 460 to 560 pixels. The cut-off for the central lobe = 55 pixels while the central peak at 54 pixels. FWHM = 1 pixels. **b** The PSF for the aperture shown in the Fig. 1b, in the range from 460 to 560 pixels. The cut-off for the central lobe = 55 pixels while the central peak at 54 pixels. FWHM = 1 pixels. **c** The PSF for the aperture shown in the Fig. 1c, in the range from 460 to 560 pixels. The cut-off for the central lobe = 55 pixels while the central peak at 54 pixels. FWHM = 1 pixels. The side lobes are strengthen compared with that shown in the figure (b). **d** The PSF for the whole aperture shown in the Fig. 1d, in the same range as in the figure (b). The cut-off for the central lobe = 57 pixels while the central peak at 54 pixels. FWHM = 3 pixels

decreased in presence of the aperture as expected for the modulating aperture.

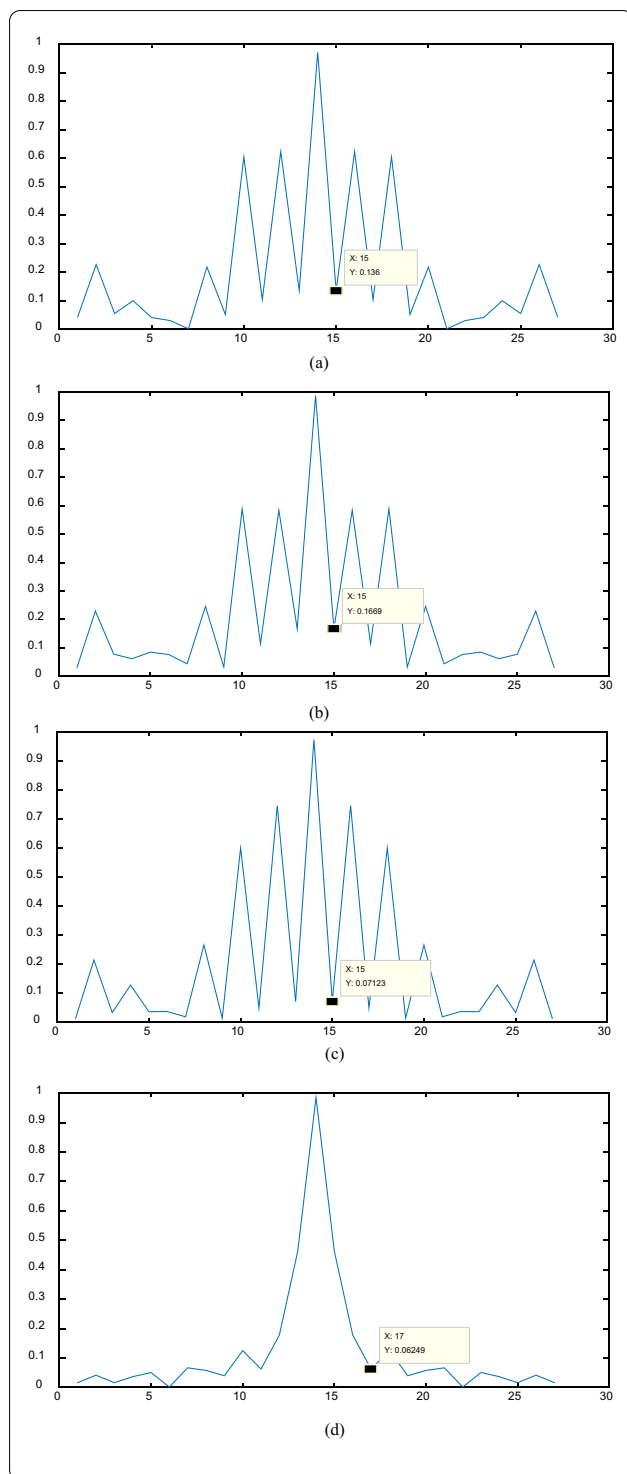
The autocorrelation of the apertures has a new shape, as shown in the Fig. 6a–C, which depends on the geometry of the aperture as compared with the known autocorrelation of square aperture giving simple triangular distribution Fig. 6d. It is shown, referring to the Fig. 6a, b, that nearly equal shapes are obtained. In addition, the center has a peak much greater than the two nearly equal side peaks.

While in the Fig. 6c, the ratio of the side peaks to the central peak is much greater than the ratio obtained in the Fig. 6a, b. This is attributed to the unequal zones shown in the Fig. 1c where the arrangement has two conjugate rectangles along x-coordinate instead of two conjugate squares as in the Fig. 6a, b.

## 5 Conclusions

The resolution computed from the FWHM showed an improvement for the suggested square apertures as compared with the uniform square aperture where the total width is kept constant. In addition, the strength of the legs in the PSF for the suggested apertures is much higher than that corresponding the uniform aperture which makes it useful for imaging of extended objects. Further increase in the legs strength is attained in the 3<sup>rd</sup> model as shown in the Fig. 2c.

A comparison of the obtained speckle image using the different apertures with that obtained in absence of the aperture showed a remarkable difference since the speckle in case of apertures resulted from the convolution product of the ordinary speckle and the PSF. In addition, the autocorrelation corresponding to the



different apertures showed a geometry related to its distribution.

We believe that the suggested apertures may be useful for imaging transparent cells in confocal microscopy since the resulted PSF is further improved as compared with the ordinary rectangular apertures.

**Fig. 3** **a** The PSF for the aperture shown in the Fig. 1a, in the range from 500 to 526 pixels. The cut-off for the central lobe = 15 pixels while the central peak at 14 pixels. FWHM = 1 pixels. **b** The PSF for the aperture shown in the Fig. 1b, in the range from 500 to 526 pixels. The cut-off for the central lobe = 15 pixels while the central peak at 14 pixels. FWHM = 1 pixels. **c** The PSF for the aperture shown in the Fig. 1c, in the range from 500 to 526 pixels. The cut-off for the central lobe = 15 pixels while the central peak at 14 pixels. FWHM = 1 pixels. The side lobes are strengthened compared with that shown in the figure (b). **d** The PSF for the whole square of dimensions 640 × 640 pixels in the same range as in the figure (c). The cut-off for the central lobe = 17 pixels while the central peak at 14 pixels. FWHM = 3 pixels

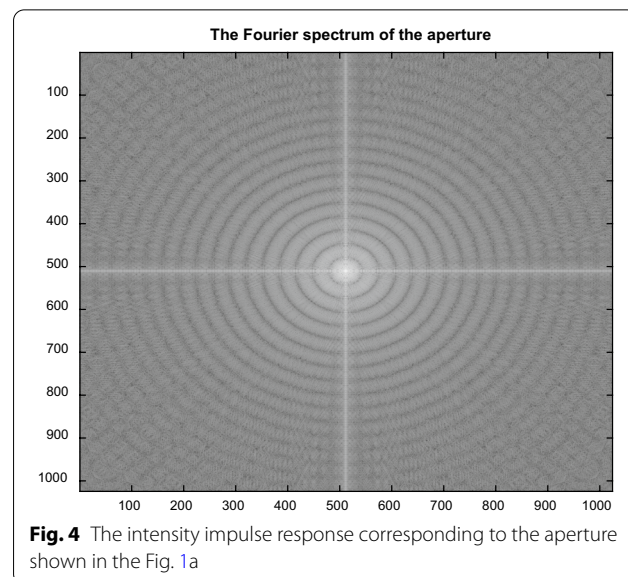


**Fig. 4** The intensity impulse response corresponding to the aperture shown in the Fig. 1a

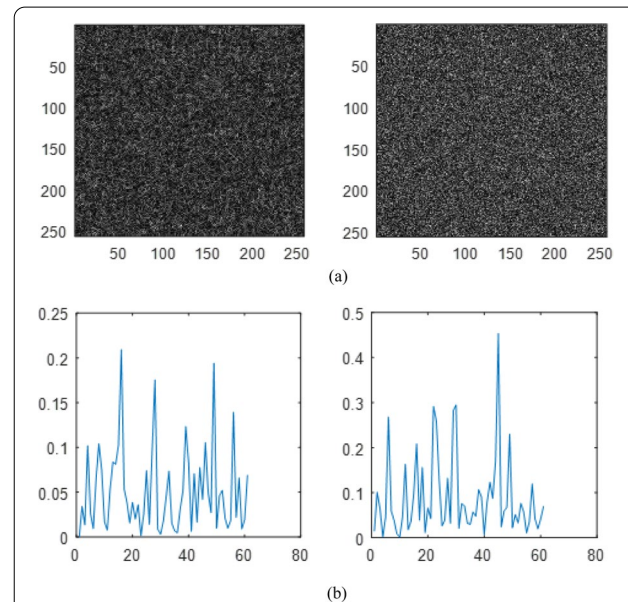


**Fig. 5** **a** In the L.H.S., speckle image in presence of the aperture shown in the Fig. 1a, while in the R.H.S., speckle image in absence of the aperture is shown. **b** In the L.H.S., speckle plot in presence of the aperture, while in the R.H.S., speckle plot in absence of the aperture is shown. The range is from 60 up to 120 pixels.



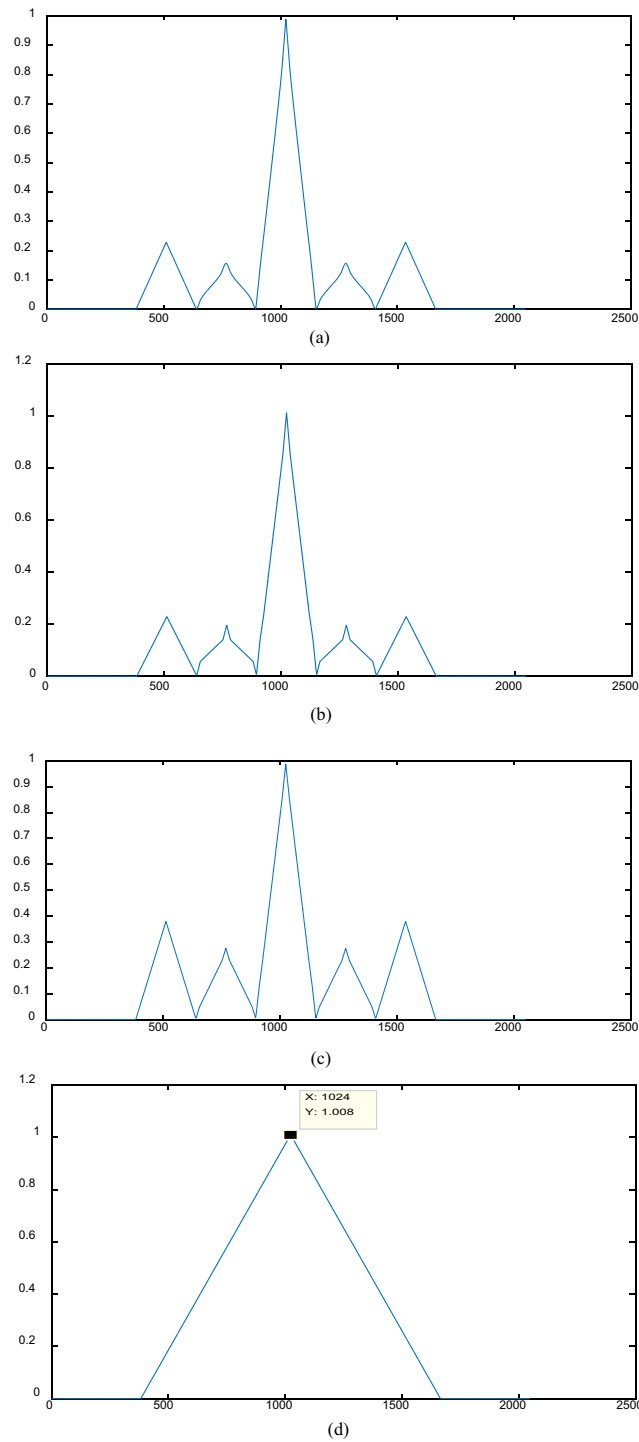


**Fig. 6** **a** The autocorrelation of the aperture shown in the Fig. 1a, where the total band width = 1280 pixels which is two times the aperture width 640 pixels. **b** The autocorrelation of the aperture shown in the Fig. 1b, where the total band width = 1280 pixels which is two times the aperture width 640 pixels. **c** The autocorrelation of the aperture shown in the Fig. 1c, where the total band width = 1280 pixels which is two times the aperture width 640 pixels. **d** The autocorrelation of the aperture shown in the Fig. 1d, where the total band width = 1280 pixels which is two times the aperture width 640 pixels

## Abbreviations

PSF: Point spread function; FWHM: Full width at half-maximum; FT.: Fourier transform; FFT: Fast Fourier transform;  $\otimes$ : Symbol for convolution operation.

## Acknowledgements

Not applicable.

## Author contributions

The corresponding author AMH has presented all steps of manuscript preparation, including the idea, the method including the theoretical analysis, and the results with discussions. TAA-S has assisted in the results and idea of rectangular formation. Both the authors read and approved the final manuscript.

## Funding

Not applicable.

## Availability of data and materials

Not applicable.

## Declarations

## Ethics approval and consent to participate

Not applicable.

## Consent for publication

Not applicable.

## Competing interests

The authors declare that they have no competing interests.

## Author details

<sup>1</sup>Physics Department, Faculty of Science, Ain Shams University, Cairo, Egypt.

<sup>2</sup>Biomedical Department, Faculty of Engineering, Helwan University, Cairo, Egypt.

Received: 15 September 2021 Accepted: 29 March 2022

Published online: 11 April 2022

## References

1. Goldfischer LI (1965) Autocorrelation function and power spectral density of laser-produced speckle patterns. *J Opt Soc Am* 55:247–253. <https://doi.org/10.1364/JOSA.55.000247>
2. Toraldo di Francia GJ (1955) Resolving power and information. *Opt Soc Am* 45:497
3. Sheppard CJR, Choudhury A (1977) Image formation in scanning microscope. *Opt Acta* 24:1051–1073
4. Sheppard CJR, Matthews HJ (1987) Imaging in high aperture optical systems. *J Opt Soc Am A* 4:1354–1360
5. Cox JJ, Sheppard CJR, Wilson T (1982) Super-resolution by confocal fluorescent microscopy. *Optik* 60:391–396
6. Sheppard CJR, Larkin KG (1994) Optimal concentration of electromagnetic radiation. *J Mod Opt* 41:1495–1505
7. Sheppard CJR, Hegedus ZS (1988) Axial behavior of pupil-plane filters. *J Opt Soc Am A* 5:643–647
8. Sheppard CJR, Choudhury A (2004) Annular pupils, radial polarization, and superresolution. *Appl Opt* 43:4322–4327
9. Sheppard CJR (2007) Filter performance parameters for high numerical aperture focusing. *Opt Lett* 32:1653–1655
10. Sheppard CJR, Martinez-Corral M (2008) Filter performance parameters for vectorial high aperture wave fields. *Opt Lett* 33:476–478
11. Sheppard CJR (2007) Fundamentals of superresolution. *Micron* 38:165–169
12. Hamed AM, Clair JJ (1983) Image and super-resolution in optical coherent microscopes. *Optik* 64:277–284
13. Hamed AM, Clair JJ (1983) Studies on optical properties of confocal scanning optical microscope using pupils with radially transmission distribution. *Optik* 65:209–218
14. Hamed AM (2017) Improvement of point spread function Optic (PSF) using linear-quadratic aperture. *Optik* 131:838–849. <https://doi.org/10.1016/j.jlleo.2016.11.201>
15. Hamed AM (2011) Discrimination between speckle images using diffusers modulated by some deformed apertures: simulations. *J Opt Eng* 50:1–7. <https://doi.org/10.1117/1.3530085>
16. Hamed AM (2019) Design of a cascaded black-linear distribution (CBLD) in circular aperture and its application on confocal laser scanning microscope (CSLM). *Am J Opt Photon* 3
17. Hamed AM (2020) Image processing of Ramses II statue using speckle photography modulated by a new Hamming-Linear aperture. *J Phys (PRAMANA)* 94:126
18. R. V. V. & Singh RK, (2016) Determining helicity and topological structure of coherent vortex beam from laser speckle. *Appl Phys Lett* 109:111108. <https://doi.org/10.1063/1.4962952>
19. Funamizu H, Uozumi J (2007) Generation of fractal speckles by means of a spatial light modulator. *Opt Express* 15:7415–7422
20. Cabezas L, Amaya D, Bolognini N, Lencina A (2015) Speckle fields generated with binary diffusers and synthetic pupils implemented on a spatial light modulator. *Appl Opt* 54:5691–5696. <https://doi.org/10.1364/AO.54.005691>
21. Zhou X, Poenar DP et al (2008) Design of MEMS devices with optical apertures for the detection of transparent biological cells. *Biomed Micro-devices* 10:639–652. <https://doi.org/10.1007/s10544-008-09175-6>
22. Salih Djilali and Behzad Ghanbari (2021) Dynamic behavior of two predators-one prey model with generalized functional response and time-fractional derivative 2021:235. <https://doi.org/10.1186/s13662-021-03395-9>
23. Boudjema I, Djilali S (2018) Turing-Hopf bifurcation in Gauss-type model with cross diffusion and its application. *Nonlinear Stud* 25(3):665–687

## Publisher's Note

Springer Nature remains neutral with regard to jurisdictional claims in published maps and institutional affiliations.